Applied Catalysis B: Environmental 156–157 (2014) 265–272

Contents lists available at ScienceDirect

Applied Catalysis B: Environmental

journal homepage: www.elsevier.com/locate/apcatb

Catalytic performance of plasma catalysis system with nickel oxide catalysts on different supports for toluene removal: Effect of water vapor

Junliang Wu[a,b], Qibin Xia[a], Haihui Wang[a], Zhong Li[a,*]

[a] School of Chemistry and Chemical Engineering, The Key Laboratory of Enhanced Heat Transfer and Energy Conservation, Ministry of Education, South China University of Technology, Guangzhou, Guangdong 510641, China
[b] School of Environment and Energy, Guangdong Provincial Key Laboratory of Atmospheric Environment and Pollution Control, South China University of Technology, Guangzhou, Guangdong 510006, China

ARTICLE INFO

Article history:
Received 20 May 2013
Received in revised form 8 March 2014
Accepted 11 March 2014
Available online 21 March 2014

Keywords:
Plasma
Catalyst
Nickel oxide
Support
Water vapor

ABSTRACT

The effect of water vapor on the performance of a combined non-thermal plasma catalysis (CPC) system with nickel oxide catalysts loaded on different supports was investigated. The catalysts NiO/γ-Al_2O_3, NiO/SBA-15 (Santa Barbara Amorphous-15), and NiO/TiO_2 were prepared and their activities were tested in the absence and presence of water vapor. Complete destruction of toluene was achieved in the absence of water vapor at ambient temperature and pressure. The activities of catalysts for the toluene conversion in dry air decreased in the following order: NiO/γ-Al_2O_3 > NiO/SBA-15 > NiO/TiO_2. The presence of water vapor in the feed stream had a significant negative impact on the performance of the CPC systems. This reduction in performance was primarily due to the quenching by water vapor of active species in the plasma and the competitive adsorption of water vapor on the catalyst surfaces. A novel *in situ* FTIR system was constructed and used to obtain *in situ* FTIR spectra of the reactive surfaces of the catalysts, revealing that the water molecules that adsorbed on the catalyst surfaces came from both water vapor present in the gas stream and from water vapor formed during the oxidation of toluene. H_2O-TPD results indicated that the activation energies of water desorption from the catalysts decreased in the following order: NiO/γ-Al_2O_3 > NiO/SBA-15 > NiO/TiO_2. The catalyst with lower water vapor desorption activation energy had higher resistance to water vapor. Therefore, the durability towards water vapor poisoning of these catalysts followed the order of: NiO/TiO_2 > NiO/SBA-15 > NiO/γ-Al_2O_3.

1. Introduction

Volatile organic compounds (VOCs) emitted from various industrial processes is an important sources of air pollution. VOCs are the precursors for the formation of photochemical smog, ground level ozone and fine particles in the air [1]. Some of air-borne VOCs have been associated with adverse health effects. For example, toluene found in gasoline, paints, glues, rubber and varnishes, causes numerous effects, including eyes and respiratory tract irritation, nausea and headaches. Therefore, considerable research attention has been focused on the removal of VOCs from the atmosphere.

Various techniques have been widely used in treating VOCs emissions from industrial plants, including carbon adsorption, catalytic oxidation, thermal decomposition, and condensation. More recently, a new technique, combined non-thermal plasma catalysis (CPC), is being developed and offers an innovative approach to solving the problem of VOCs pollution, especially when present in low concentrations [2]. A CPC system has the advantage of operating at ambient temperature and pressure. In the CPC system, solid catalysts are often placed inside the non-thermal plasma zone [3], where catalytic reactions can be induced by the plasma without external heating. VOCs are quickly oxidized under ambient conditions through the synergetic effect of the combination of the plasma and catalyst [4]. A catalyst plays an important role in determining the overall efficiency of VOCs removal in the CPC system [5,6]. Khacef et al. [7] tested Ag, Au, Cu, and Co catalysts supported on Al_2O_3 for toluene decomposition in a catalytic dielectric barrier discharge (DBD) reactor and found that Au/Al_2O_3 had the highest level of toluene removal. Zhao et al. [8] applied a cycled storage-discharge (CSD) plasma catalytic process using HZSM-5, Ag/HZSM-5, Cu/HZSM-5 and AgCu/HZSM-5 catalysts to remove low concentrations of formaldehyde, and reported that AgCu/HZSM-5

* Corresponding author. Fax: +86 20 87110608.
E-mail address: cezhli@scut.edu.cn (Z. Li).

http://dx.doi.org/10.1016/j.apcatb.2014.03.017
0926-3373/

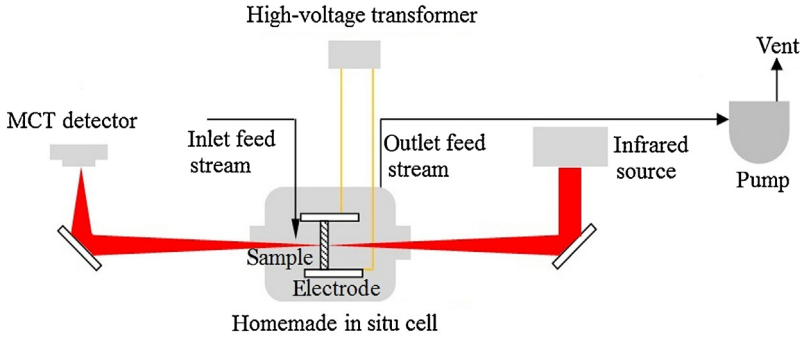

Fig. 1. Scheme of setup for FTIR measurements with a custom-made *in situ* cell.

performed best. Karuppiah et al. [9] used a non-thermal plasma rector with a catalytic electrode modified with Mn and Co oxides to oxidize isopropanol and found that MnOx performed better than CoOx.

The nickel catalyst is an important catalyst for complete oxidation of VOCs [10]. Kim et al. [11] demonstrated that benzene conversion in a CPC system using Ni/TiO_2 was higher than when using Ag/TiO_2. Ogata et al. [12] also reported that $NiO/\gamma\text{-}Al_2O_3$ showed good performance for VOCs decomposition in plasma.

In recent years, it has been noticed that the presence of water vapor in the gas stream may affect the performance of the CPC systems. Fan et al. [13] investigated the effects of relative humidity (30%, 50% and 80%) on the removal of low concentration of benzene in air by a CPC system fitted with a $MnOx/Al_2O_3$ catalyst and found that increasing humidity inhibited the production of O_3 in plasma, thus reducing the benzene conversion. Guo et al. [14] studied the effect of relative humidity on toluene removal using a $MnOx/Al_2O_3$/nickel foam catalyst in the plasma and found that toluene removal decreased with increased humidity. Thevenet et al. [15] investigated the influence of water vapor on acetylene oxidation in a CPC system with a TiO_2 catalyst and reported that the presence of water vapor in the gas stream greatly reduced the removal of acetylene. Van Durme et al. [16] studied the abatement of toluene in indoor air using a CPC system fitted with TiO_2, and found that for an inlet gas stream with 27% relative humidity, the degradation of toluene was only 40% of the decomposition observed in the absence of water.

In each of these previous studies, only one catalyst was included. From our perspective, different supports for the metal oxide catalysts could have different susceptibilities to water vapor. Therefore, this study was undertaken to examine the effect of water vapor on the performance of a CPC system with nickel oxide catalysts loaded on different supports, with the aim of widening the utility of the CPC systems in practical situations.

In this work, three types of the nickel based catalysts with different supports – $\gamma\text{-}Al_2O_3$, SBA-15 and TiO_2 – were prepared using an impregnation method. The catalysts were evaluated and characterized under both dry and moist conditions. The effects of different supports and water vapor on the activities of catalysts for the toluene conversion are discussed and reported below.

2. Experimental

2.1. Catalyst preparation

Three different materials – $\gamma\text{-}Al_2O_3$, SBA-15 and TiO_2 (40–60 mesh) – were used as the supports. The $\gamma\text{-}Al_2O_3$ and TiO_2 were supplied by Alfa Aesa; and the SBA-15 was supplied by Shanghai Novel Chemical Technology Company, China. Nickel oxide catalysts were prepared by impregnation using $Ni(NO_3)_2$ aqueous solutions, followed by drying for 24 h at 30 °C. The samples were then heated to 120 °C for 1 h and calcined in air at 400 °C for 3 h. The resulting catalysts contained 5 wt% nickel loadings and were denoted as $NiO/\gamma\text{-}Al_2O_3$, NiO/SBA-15, and NiO/TiO_2.

2.2. Catalyst characterization

X-ray diffraction (XRD) patterns were measured with a Bruker D8 Advance diffractometer using Cu Kα radiation. The X-ray tube was operated at 40 kV and 40 mA.

Hydrogen temperature programmed reduction (H_2-TPR) was performed in a Micromeritics Autochem 2920 instrument. The gas mixture (10% H_2 and 90% Ar) was passed through the catalyst sample (0.05 g) at a flow rate of 30 ml/min while the temperature was increased from room temperature to 800 °C at a heating rate of 10 °C/min.

Carbon monoxide temperature programmed desorption (CO-TPD) was employed to estimate the dispersion of the active component of the catalyst [17]. CO-TPD was measured in a Micromeritics AutoChem 2920 instrument. The samples were reduced in a flow of 10% H_2/Ar (30 ml/min) at 650 °C for 1 h, and then flushed with pure helium flow (30 ml/min) for 0.5 h at the same temperature. After being cooled to room temperature, the samples were exposed for 2 h to a gas flow of 99.99% CO. The samples were then heated to 650 °C in pure helium flow (10 ml/min) at a heating rate of 5 °C/min. The desorbed gas was analyzed with a thermal conductivity detector (TCD).

Water temperature programmed desorption (H_2O-TPD) experiments were conducted at different heating rates of 2–6 °C/min. In each experiment, the sample that had adsorbed water vapor was packed in a quartz tube and then heated in a flow of high-purity N_2 at a constant rate of 10 ml/min. The desorbed water vapor was measured in a Micromeritics Autochem 2920 instrument equipped with a TCD. The effluent curves (also known as TPD curves) were recorded. The experimental procedures have been reported in detail elsewhere [18–20].

In situ Fourier transform infrared (*in situ* FTIR) spectra were recorded using a Nicolet 6700 spectrometer equipped with a mercury-cadmium-telluride (MCT) detector cooled by liquid nitrogen. A custom-made flow cell with a path length of 10 cm and capped at both ends by IR-transparent KBr windows was used for the *in situ* measurements (Fig. 1). Two copper sheets separated by quartz glass plates acted as the electrodes. The discharge gap was 4 mm. An applied voltage of 8000 V was supplied by a high-voltage transformer (50 Hz). The calculated electric field intensity in the discharge gap was 20 kV/cm. A 10 mg sample of catalyst was pressed into a wafer that was approximately 1 cm in diameter. After being placed in a sample holder between the electrodes, the sample was heated to 300 °C for 1 h in pure Ar before measurements. Then, the gas steam (10 ml/min) containing 0.8 vol% water vapor

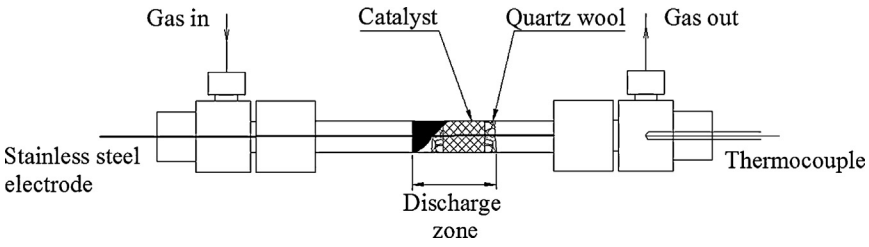

Fig. 2. Schematic of the DBD plasma reactor.

and 150 mg/m^3 (i.e., 37 ppm) toluene flowed through the cell for 2 h and allowed to equilibrate at 40 °C. The spectra sampling interval was 24.37 s, and all spectra used data accumulated from 64 scans at a resolution of 4 cm^{-1}.

2.3. Catalytic evaluation

Catalytic activity tests were performed in a DBD reactor operated at a temperature of 40 °C at atmospheric pressure. The reactor (Fig. 2), consisted of two coaxial electrodes separated by a quartz tube (o.d. = 7.8 mm, i.d. = 6.0 mm). A stainless steel high-voltage electrode (1.0 mm in diameter) was positioned in the center of the tube as the inner electrode. Aluminum foil wrapped on the outer surface of the tube acted as the outer electrode. The discharge length was 30 mm, and the discharge gap was 2.5 mm. A high-voltage transformer (50 Hz) provided the energy for the plasma. The applied voltage and current of the reactor were measured by a high-voltage probe and a μA meter. The discharge power was the product of the applied voltage and the current. Specific input energy (SIE) was calculated from the following expression:

$$\mathrm{SIE(J/l)} = \frac{\text{Discharge power(W)}}{\text{Gas flow rate(l/ min)}} \times 60(\mathrm{s/\ min}) \quad (1)$$

A toluene–air mixture (150 mg/m^3) was passed through the reactor at a flow rate of 100 ml/min. The catalysts with the same volume were positioned at the end of the plasma zone, supported by quartz wool. The masses of NiO/γ-Al_2O_3, NiO/SBA-15 and NiO/TiO_2 were 0.17 g, 0.15 g, and 0.27 g, respectively. The temperature change in the gas flow during the reaction was measured with a thermocouple located at the outlet of the reactor. In all of the experiments, the maximum temperature rise in the gas flow was only 1–2 °C; i.e., any effects observed were the result of non-thermal processes. The effluent was analyzed by an on-line gas chromatography, using a Shanghai Hu'ai GC960 chromatograph equipped with a flame ionization detector.

Toluene conversion rate and CO_2 selectivity were defined as follows:

$$\text{Toluene conversion rate}(\%) = \frac{[\text{toluene}]_{\text{inlet}} - [\text{toluene}]_{\text{outlet}}}{[\text{toluene}]_{\text{inlet}}} \times 100\% \quad (2)$$

$$\mathrm{CO_2\ selectivity}(\%) = \frac{[\mathrm{CO_2}]}{[\mathrm{CO_2}] + [\mathrm{CO}]} \times 100\% \quad (3)$$

where [CO_2], [CO] and [toluene] are CO_2, CO and toluene concentrations (ppm), respectively.

3. Results and discussion

3.1. Catalytic activity evaluation in dry air

Fig. 3 shows the decomposition of toluene in the CPC systems with nickel based catalysts and in the plasma system without a catalyst as a function of SIE. As expected, the toluene conversion increased with increasing SIE in all cases. For the plasma system without a catalyst, the toluene conversion increased from 28.6% to 68.0% when SIE increased from 2.16 to 4.80 J/l. For the CPC systems, the toluene conversions were 76.0–100%, 46.6–98.4% and 42.3–96.0% for NiO/γ-Al_2O_3, NiO/SBA-15, and NiO/TiO_2, respectively, over the same change in SIE. The higher SIE could result in an increase in the amounts and the mean energy of energetic electrons, thereby leading to increased amounts of various oxidative species due to collision between gas molecules and the energetic electrons. As a result, the toluene conversion was increased.

Fig. 3 exhibits that toluene conversion of the CPC systems was significantly higher than the plasma system without a catalyst. It meant that synergy of non-thermal plasma and catalyst can enhance the toluene conversion with an increment of approximately 30–40%. In the CPC systems, synergetic effects are mainly related to the activation of the catalyst by the plasma. Activation mechanisms of catalysts include ozone, UV, local heating, changes in work function, activation of lattice oxygen, adsorption/desorption, and direct interaction of gas phase radicals with the catalyst surface and the adsorbed molecules etc. [21].

In addition, the toluene conversions of the CPC systems with different catalysts were different. Fig. 3 shows that at the same SIE, the toluene conversion of the CPC system with NiO/γ-Al_2O_3 was the highest, while that of the CPC system with NiO/TiO_2 was the lowest. The activities of these three catalysts decreased in the following order: NiO/γ-Al_2O_3 > NiO/SBA-15 > NiO/TiO_2. The difference in catalytic performance possibly reflects the differences in the dispersion of NiO on the different supports, which will be confirmed by catalyst characterization in Section 3.2.

Both the CPC systems and the plasma system without a catalyst gave high toluene conversion with very low energy consumption. The SIE applied in our system was in the range of 2–5 J/l, being much lower than the SIE of tens to hundreds J/l reported in the previous works [5]. The energy efficiency of this CPC system

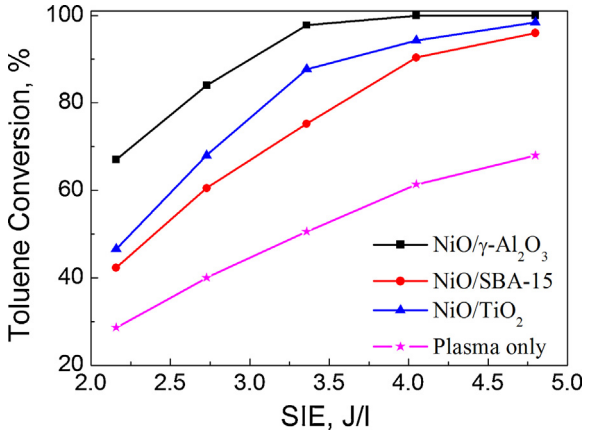

Fig. 3. Toluene conversion of the CPC systems and the plasma system without a catalyst as a function of SIE (temperature = 40 °C; inlet toluene concentration = 150 mg/m^3; dry air).

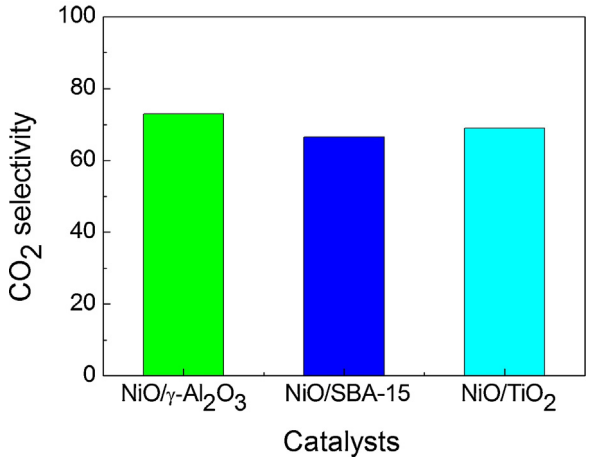

Fig. 4. CO_2 selectivity of the CPC systems with different catalysts (temperature = 40 °C; inlet toluene concentration = 150 mg/m^3; SIE = 4.8 J/l; dry air).

was up to 105.0–112.5 g/kWh, which was much higher than those (<50 g/kWh) reported in the previous works [4]. This improvement can be ascribed to the special structure design of the plasma reactor which has a small discharge gap distance and uses thin dielectric materials. The smaller discharge gap distance and the thinner dielectric materials can produce stronger electric field. The stronger electric field increased the amounts and the mean energy of the energetic electrons, leading to the increase in the amounts of various oxidative species, and thus increased the toluene conversion.

The end-products were analyzed in order to evaluate the CO_2 selectivity of the systems. The main products were CO_2 and CO, with only trace amounts of hydrocarbons being detected at the reactor outlet. In addition, as reported in previous work [22], trace amounts of residue on the catalyst surfaces after the reaction were also observed. Therefore, COx was considered as the main end-products. Fig. 4 shows the CO_2 selectivity of the CPC systems with different catalysts. The CO_2 selectivity was approximately 70% for each of the catalysts; i.e. the different support materials had an insignificant effect on CO_2 selectivity. The CO_2 selectivity of the CPC systems with metal oxide catalysts was still lower than that with noble metal catalysts [11]. This behavior might result from a more accumulation of chemisorbed oxygen species on the surface of noble metal catalysts compared to the metal oxide catalysts [23].

3.2. Characterization of the catalysts

3.2.1. XRD analysis of the catalysts

Fig. 5 shows XRD patterns of NiO on different supports, i.e., γ-Al_2O_3, SBA-15 and TiO_2. In the cases of NiO/SBA-15 and NiO/TiO_2, weak diffraction peaks of NiO (JCPDS 47-1049) were observed at $2\theta = 43°$, suggesting that NiO crystallite was present in both cases. For the NiO/γ-Al_2O_3 catalyst, no such featured peak of NiO crystalline was observed. This observation suggested that the crystallite size of nickel oxide on the γ-Al_2O_3 support was so small that it was beyond the detection limit of XRD. These data suggested a more dispersed nickel oxide on the γ-Al_2O_3 support.

3.2.2. H_2-TPR studies

Fig. 6 displays a comparison of TPR profiles of the three catalysts, whose reduction temperatures differed. The TPR profile for NiO/γ-Al_2O_3 showed one broad peak at 576 °C with a shoulder at 720 °C. The 576 °C peak was ascribed to the strong interaction of highly dispersed clusters of NiO with the γ-Al_2O_3 support, while the shoulder at 720 °C was attributed to the reduction of $NiA1_2O_4$ [24,25]. These data indicated that the NiO was highly dispersed as clusters of NiO or nickel ions in the γ-Al_2O_3 support [26]. The TPR profile for the NiO/SBA-15 catalyst showed one broad peak at 463 °C with a small shoulder at 375 °C. The 375 °C shoulder was

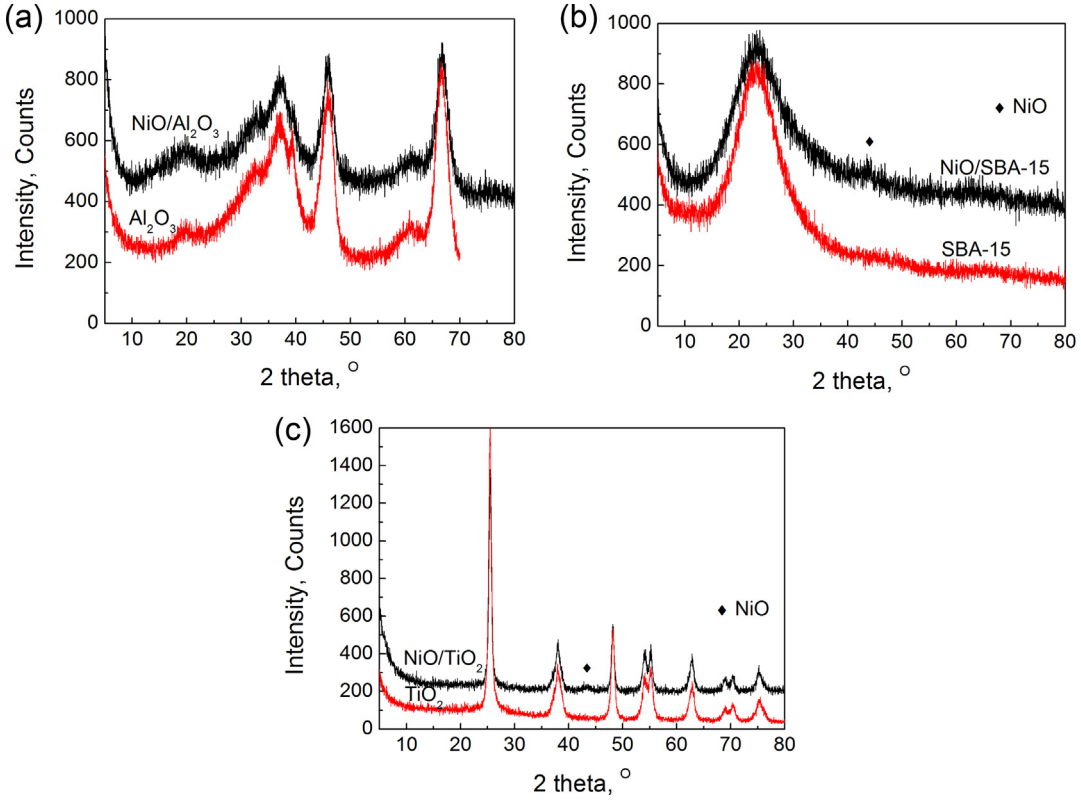

Fig. 5. XRD patterns of the freshly prepared nickel based catalysts.

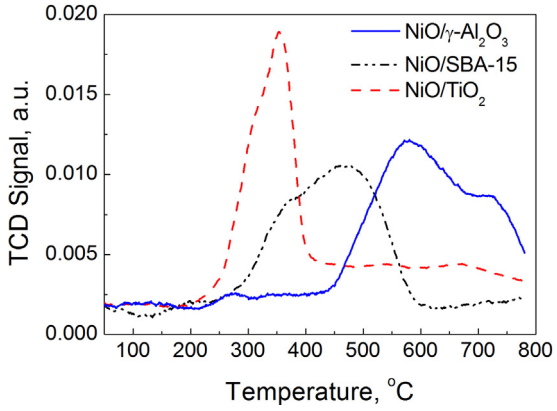

Fig. 6. H_2-TPR profiles of the freshly prepared nickel based catalysts.

associated with the reduction of bulk NiO, and the peak at 463 °C was as a result of the reduction of NiO that was strongly interacting with the SBA-15 [27,28]. This TPR response meant that most of the supported NiO was present as highly dispersed NiO, and a smaller portion was present as bulk NiO. The TPR profile for the NiO/TiO_2 catalyst exhibited only one pronounced reduction peak at 353 °C, which was assigned to the reduction of bulk NiO [29], suggesting that the supported NiO was mainly present as bulk NiO. In short, this analysis indicated that the extent of NiO dispersion of these three catalysts decreased in the following order: $NiO/\gamma\text{-}Al_2O_3$ > NiO/SBA-15 > NiO/TiO_2, which is the same the order of activities of these three catalysts seen above.

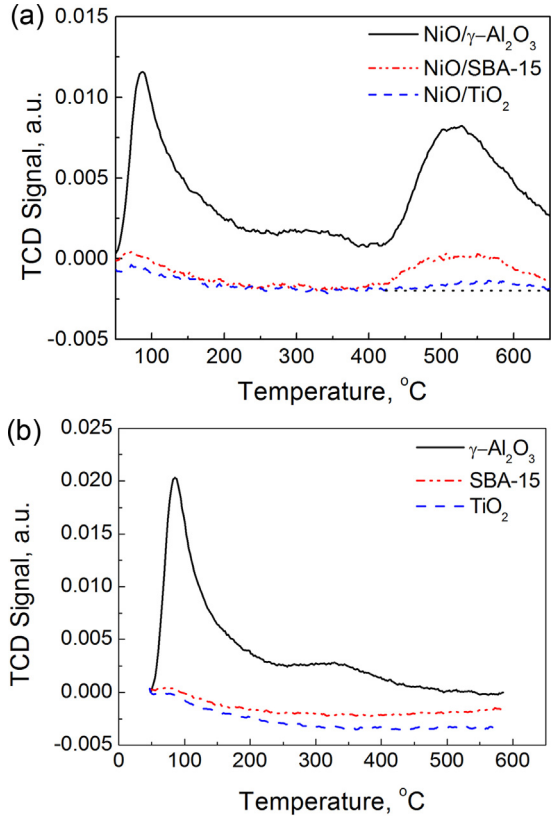

Fig. 7. CO-TPD spectra of the freshly prepared nickel based catalysts (a) and the supports (b).

3.2.3. CO-TPD studies

Fig. 7(a) shows the CO-TPD spectra of the three catalysts, and Fig. 7(b) gives CO-TPD spectra of the three supports for comparison. In Fig. 7(a), the desorption peaks of CO were observed above 400 °C. These peaks corresponded to the desorption of CO chemisorbed on reduced Ni atoms. The area under the desorption peaks was directly proportional to the amounts of desorbed CO. Assuming a stoichiometry of one CO molecule per surface metal atom, (i.e., CO/Ni = 1), this measurement is a reasonable estimation of the Ni dispersion [30]. Therefore, the areas of these desorption peaks (and their presumptive dispersion) for three catalysts decreased in the following order: $NiO/\gamma\text{-}Al_2O_3$ > NiO/SBA-15 > NiO/TiO_2, in good agreement with the trend in catalytic activity observed in Fig. 3. The data are consistent with the higher NiO dispersion on the support being correlated with higher catalytic activity for toluene conversion in the CPC system.

3.3. The inhibiting effect of water vapor on toluene conversion in the CPC system

3.3.1. Catalytic activity evaluation in humid air

Fig. 8 shows the effects of water vapor concentration on toluene conversion of the CPC systems with nickel based catalysts. The presence of water vapor had negative, dose-dependent influence on the performance of each catalyst in the CPC systems. There are two possible reasons for this behavior. Firstly, the addition of water vapor could change the plasma discharge characteristic. When water vapor covered the dielectric, it reduced the surface resistance and increased the effective dielectric capacity. Therefore, it decreased total current in the system [31], and the numbers of electrons. When the concentration of water vapor increased, the probability of reactions between water molecules and energetic electrons increased. The more energetic electrons would be quenched by electronegative water molecules, which would lower the electron density and average energy of the system, thereby decreasing the amount of active chemical species [15,32]. Secondly, the presence of water vapor would decrease the number of the active sites available for toluene and O_3 adsorption due to the competitive adsorption of water vapor on the catalyst surfaces.

In addition, as shown in Table 1, the sensitivity to the presence of water vapor varied among the catalysts. Under similar conditions, the $NiO/\gamma\text{-}Al_2O_3$ was more sensitive to poisoning by water vapor than the other two catalysts. For example, the $NiO/\gamma\text{-}Al_2O_3$ displayed the highest toluene conversion in dry air at a SIE of 4.80 J/l (100%). However its catalytic activity was the lowest of the three catalysts when the water vapor concentration was 4.43 vol% (22.0%). In short, impact of water vapor on the performance of the catalyst decreased in the order of $NiO/\gamma\text{-}Al_2O_3$ > NiO/SBA-15 > NiO/TiO_2.

3.3.2. Desorption activation energies of water vapor on the catalysts studies

The H_2O-TPD method was used to determine how strongly molecules were bound to the surfaces of the supports [18]. Fig. 9 shows the H_2O-TPD curves of water desorption on the three catalysts at different heating rates. There was a clear peak in each TPD

Table 1
The effect of water vapor concentration on toluene conversion of the CPC systems.

Catalyst	Toluene conversion		Percentage reduction
	In the absence of water vapor	In the presence of water vapor	
$NiO/\gamma\text{-}Al_2O_3$	100%	22.0%	78.0%
NiO/SBA-15	98.4%	41.0%	57.4%
NiO/TiO_2	96.0%	47.6%	48.4%

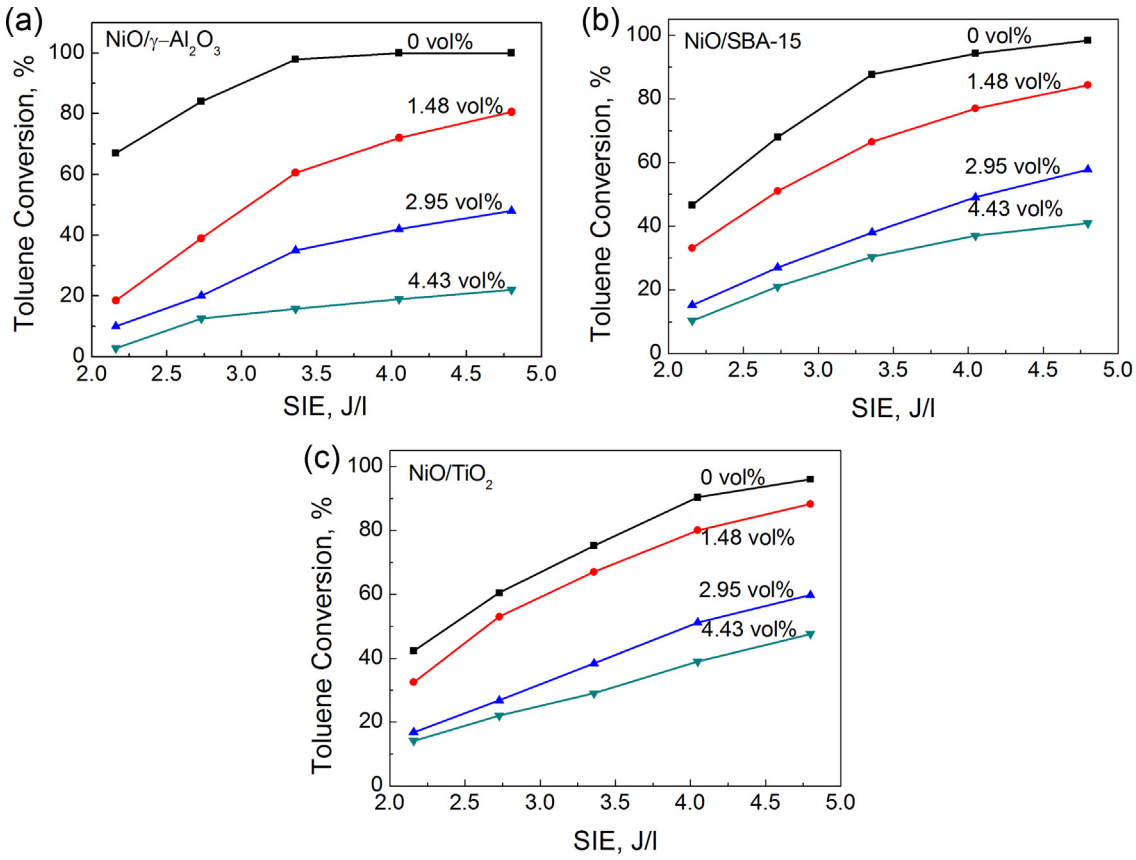

Fig. 8. Effects of water vapor concentration on toluene conversion in the CPC system with nickel based catalysts (temperature = 40 °C; inlet toluene concentration = 150 mg/m^3).

curve due to desorption of water vapor. The peak temperature T_p increased with an increase in the heating rate (see Table 2).

The desorption activation energy, E_d, of water vapor can be estimated from a series of T_p values obtained at different heating rates [18–20]. The results are also listed in Table 2. Generally, the greater desorption activation energy, the stronger interaction between water molecules and the catalyst surfaces. The data in Table 2 show that the E_d of water vapor on the catalysts followed the order: NiO/γ-Al_2O_3 > NiO/SBA-15 > NiO/TiO_2. This result implies that the competitive adsorption of water vapor is stronger on NiO/γ-Al_2O_3 than on the other two catalysts. The stronger competitive adsorption of water vapor on the surfaces of the catalyst results in the greater reduction in activity. Thus, the durability towards water vapor poisoning of these catalysts exhibited the following order: NiO/TiO_2 > NiO/SBA-15 > NiO/γ-Al_2O_3.

3.3.3. *In situ FTIR studies*

An *in situ* FTIR system was constructed (Fig. 1), which made it possible to collect *in situ* FTIR data to provide continuous monitoring of surface-adsorbed species. This information gives new insight on the role of water vapor during the plasma catalysis reaction. Fig. 10 shows a set of FTIR spectra obtained during the plasma catalysis oxidation of toluene on the NiO/γ-Al_2O_3 catalyst with and without water vapor in the feed stream.

Under dry condition, before discharge, the FTIR spectrum showed very weak peaks that are assigned to the adsorption of toluene, with the flat and broad band in the 3600–3200 cm^{-1} region assigned to bridging OH groups H-bonded with toluene [33]. After discharge for 20 min without water vapor, the intensity of peaks at 3640 cm^{-1}, 3600–3200 cm^{-1}, 1640 cm^{-1} increased. The peak at 3640 cm^{-1} was assigned to a lattice OH stretching mode, which arose from the vibration of firmly bounded H_2O. The strong broad band at 3600–3200 cm^{-1} was related to hydrogen-bonded OH stretching vibrations. The peak at 1640 cm^{-1} was associated with the H_2O of crystallization bending vibration [34,35]. The increasing intensity of these peaks was attributed to water produced during toluene oxidation reaction. In addition, the peaks at 1597 cm^{-1} and 1393 cm^{-1} were assigned to functional group vibrations of organic intermediate products on the surfaces of the catalyst, including benzoic acid, benzaldehyde, and benzyl alcohol [36,37].

Under humid condition, before discharge and after adsorption equilibrium of water vapor on the catalyst surfaces, the FTIR spectra show that the intensity of the peaks at 3640 cm^{-1}, 3600–3200 cm^{-1} and 1640 cm^{-1} related to H_2O grew sharply due to the adsorption

Table 2
Desorption activation energy, E_d, of water vapor on three catalysts.

Catalyst	The peak temperature T_p of TPD curves at different heating rates (°C)					Desorption activation energy E_d (kJ/mol)
	2 °C/min	3 °C/min	4 °C/min	5 °C/min	6 °C/min	
NiO/γ-Al_2O_3	329.7	336.0	340.2	343.8	346.0	64.0
NiO/SBA-15	327.7	332.9	336.6	340.2	342.2	57.6
NiO/TiO_2	323.3	331.5	336.1	340.2	341.9	47.4

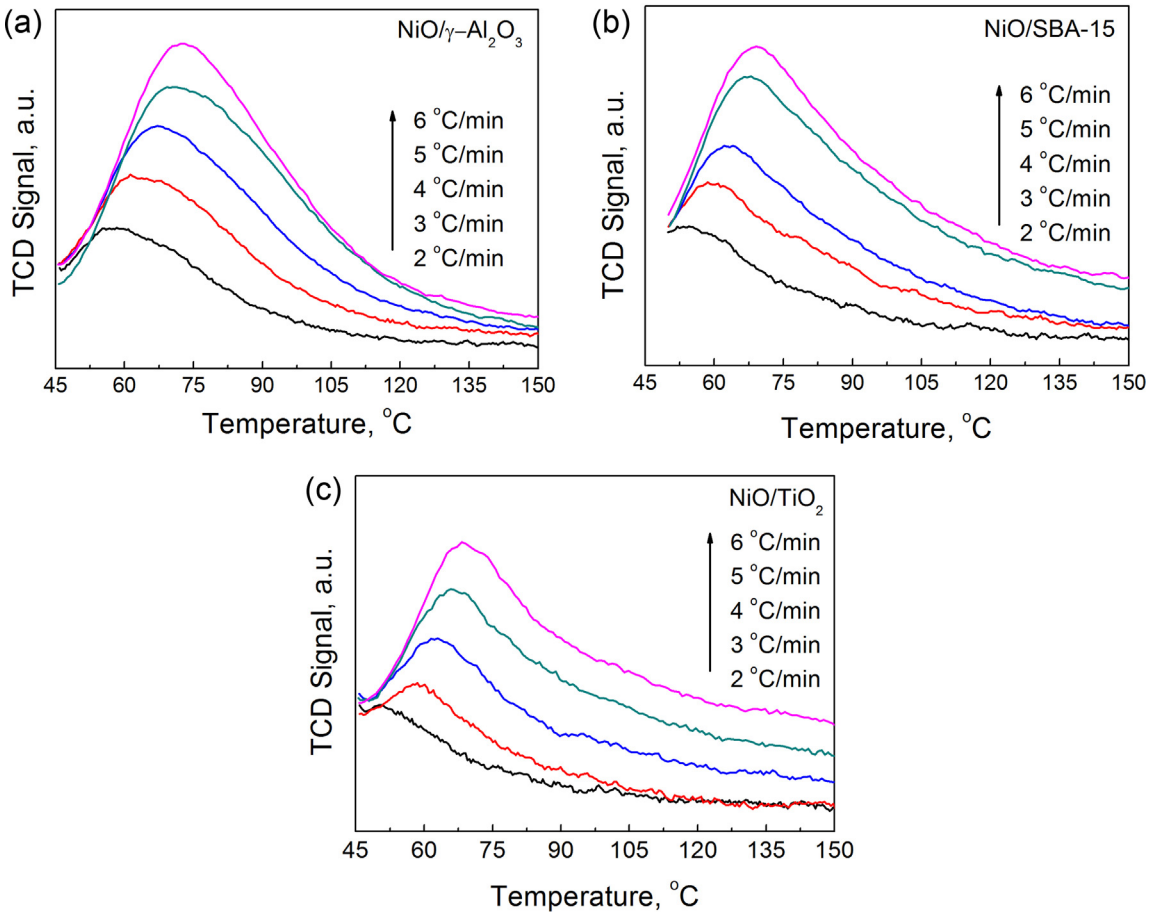

Fig. 9. H_2O-TPD curves of the nickel based catalysts.

of water vapor. After discharge, the intensity of the peaks still increased slightly with time, which meant that the amount adsorbed of water vapor on the surfaces slightly increased with reaction time. The increased amount of adsorbed water vapor might also come from toluene oxidation. Similar observations were also seen in the spectra of NiO/SBA-15 and NiO/TiO_2.

The foregoing results demonstrate that the application of *in situ* FTIR can provide direct evidence of water vapor adsorption on the surfaces of the catalysts during the reaction. It revealed that there were three kinds of water presented on the catalyst surfaces; i.e. lattice OH (firmly bounded H_2O), hydrogen-bonded OH, and crystallization H_2O. This information may be helpful in guiding the preparation of hydrophobic supported catalysts in future.

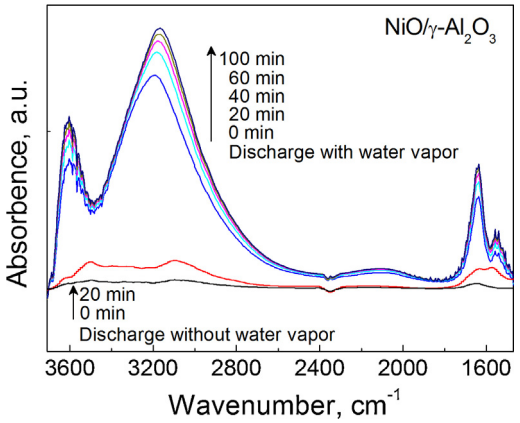

Fig. 10. *In situ* FTIR spectra of the $NiO/\gamma\text{-}Al_2O_3$ catalyst in plasma with and without water vapor in feed stream (temperature = 40 °C; inlet toluene concentration = 150 mg/m^3; water vapor concentration = 0.8 vol%).

4. Conclusion

Complete decomposition of toluene was achieved by a CPC system with nickel based catalysts under conditions of dry air and ambient temperature. The activities of the three nickel based catalysts in dry air decreased in the following order: $NiO/\gamma\text{-}Al_2O_3$ > NiO/SBA-15 > NiO/TiO_2. These results were attributed to the different extent of NiO dispersion on these three supports. The higher NiO dispersion results in higher activity of the supported catalyst. The presence of water vapor had a significant negative impact on the activities of the catalysts due to the quenching of reactive species and competitive adsorption of water vapor on the surface active sites of the catalysts. H_2O-TPD experiments showed that the desorption activation energies of water vapor on the catalysts decreased in the following order: $NiO/\gamma\text{-}Al_2O_3$ > NiO/SBA-15 > NiO/TiO_2, which indicated that the order of water vapor resistance of these supported catalysts decreased in the following order: NiO/TiO_2 > NiO/SBA-15 > $NiO/\gamma\text{-}Al_2O_3$. The application of *in situ* FTIR spectroscopy provided direct evidence of water vapor adsorption on the catalyst surfaces during the reaction. This information may be helpful in guiding the selection and/or design of appropriate catalysts to further improve the performance of the CPC systems for VOCs removal in future.

Acknowledgements

This work was supported by National Natural Science Foundation of China (No. 20936001), National Science Fund for Distinguished Young Scholars of China (No. 21225625), the Science Foundation of Guangdong Province, the State Key Lab of Subtropical Building Science, South China University of Technology (Grant C713001Z), and the Fundamental Research Funds for the Central Universities. We are grateful to Dr. Donald G. Barnes and Dr. Jing Xiao for providing helpful advice to improve our paper.

References

[1] Y. Liu, M. Shao, L.L. Fu, S.H. Lu, L.M. Zeng, D.G. Tang, Atmos. Environ. 42 (2008) 6247–6260.
[2] H.B. Huang, D.Y.C. Leung, J. Catal. 280 (2011) 60–67.
[3] A. Baylet, P. Marécot, D. Duprez, X. Jeandel, K. Lombaert, J.M. Tatibouët, Appl. Catal. B-Environ. 113–114 (2012) 31–36.
[4] J. Van Durme, J. Dewulf, C. Leys, H. Van Langenhove, Appl. Catal. B-Environ. 78 (2008) 324–333.
[5] A.M. Vandenbroucke, R. Morent, N. De Geyter, C. Leys, J. Hazard. Mater. 195 (2011) 30–54.
[6] H.L. Chen, H.M. Lee, S.H. Chen, M.B. Chang, S.J. Yu, S.N. Li, Environ. Sci. Technol. 43 (2009) 2216–2227.
[7] H. Than Quoc An, T. Pham Huu, T. Le Van, J.M. Cormier, A. Khacef, Catal. Today 176 (2011) 474–477.
[8] D.Z. Zhao, X.S. Li, C. Shi, H.Y. Fan, A.M. Zhu, Chem. Eng. Sci. 66 (2011) 3922–3929.
[9] J. Karuppiah, L. Sivachandiran, R. Karvembu, Ch. Subrahmanyam, Chem. Eng. J. 165 (2010) 194–199.
[10] M. Stoyanova, P. Konova, P. Nikolov, A. Naydenov, St. Christoskova, D. Mehandjiev, Chem. Eng. J. 122 (2006) 41–46.
[11] H.H. Kim, A. Ogata, S. Futamura, IEEE Trans. Plasma Sci. 34 (2006) 984–995.
[12] A. Ogata, H. Einaga, H. Kabashima, S. Futamura, S. Kushiyama, H.H. Kim, Appl. Catal. B-Environ. 46 (2003) 87–95.
[13] X. Fan, T.L. Zhu, Y.J. Wan, X. Yan, J. Hazard. Mater. 180 (2010) 616–621.
[14] Y.F. Guo, X.B. Liao, J.H. He, W. Ou, D.Q. Ye, Catal. Today 153 (2010) 176–183.
[15] F. Thevenet, O. Guaitella, E. Puzenat, C. Guillard, A. Rousseau, Appl. Catal. B-Environ. 84 (2008) 813–820.
[16] J. Van Durme, J. Dewulf, W. Sysmans, C. Leys, H. Van Langenhove, Appl. Catal. B-Environ. 74 (2007) 161–169.
[17] E. van Steen, E.L. Viljoen, J. van de Loosdrecht, M. Claeys, Appl. Catal. A-Gen. 335 (2008) 56–63.
[18] H.Y. Pan, M.Y. Xu, Z. Li, S.S. Huang, C. He, Chemosphere 76 (2009) 721–726.
[19] Z.X. Zhao, X.M. Li, S.S. Huang, Q.B. Xia, Z. Li, Ind. Eng. Chem. Res. 50 (2011) 2254–2261.
[20] Z.J. Zhang, S.K. Xian, H.X. Xi, H.H. Wang, Z. Li, Chem. Eng. Sci. 66 (2011) 4878–4888.
[21] H.H. Kim, A. Ogata, S. Futamura, Appl. Catal. B-Environ. 79 (2008) 356–367.
[22] J. Karuppiah, E. Linga Reddy, P. Manoj Kumar Reddy, B. Ramaraju, R. Karvembu, Ch. Subrahmanyam, J. Hazard. Mater. 237–238 (2012) 283–289.
[23] M. Magureanu, D. Piroi, N.B. Mandache, V.I. Pârvulescu, V. Pârvulescu, B. Cojocaru, C. Cadigan, R. Richards, H. Daly, C. Hardacre, Appl. Catal. B-Environ. 104 (2011) 84–90.
[24] A.J. Akande, R.O. Idem, A.K. Dalai, Appl. Catal. A-Gen. 287 (2005) 159–175.
[25] C.P. Li, Y.W. Chen, Thermochim. Acta 256 (1995) 457–465.
[26] R. Molina, G. Poncelet, J. Catal. 173 (1998) 257–267.
[27] N. Wang, W. Chu, T. Zhang, X.S. Zhao, Int. J. Hydrogen Energy 37 (2012) 19–30.
[28] D.P. Liu, X.Y. Quek, H.H. Adeline Wah, G.M. Zeng, Y.D. Li, Y.H. Yang, Catal. Today 148 (2009) 243–250.
[29] Y. Xu, J.Q. Ma, Y.F. Xu, H. Li, H.X. Li, P. Li, X.G. Zhou, Appl. Catal. A-Gen. 413–414 (2012) 350–357.
[30] A. Tanksale, J.N. Beltramini, J.A. Dumesic, G.Q. Lu, J. Catal. 258 (2008) 366–377.
[31] Z. Falkenstein, J.J. Coogan, J. Phys. D: Appl. Phys. 30 (1997) 817–825.
[32] A.A. Sarani, Yu. Nikiforov, C. Leys, Phys. Plasma 17 (2010) 063504.
[33] X.Y. Li, X.J. Zou, Z.P. Qu, Q.D. Zhao, L.Z. Wang, Chemosphere 83 (2011) 674–679.
[34] B.H. Aristizábal, C.M. de Correa, A.I. Serykh, C.E. Hetrick, M.D. Amiridis, Microp. Mesopor. Mater. 112 (2008) 432–440.
[35] H.A. Al-Abadleh, V.H. Grassian, Langmuir 19 (2003) 341–347.
[36] B. Hauchecornea, D. Terrens, S. Verbruggen, J.A. Martens, H. Van Langenhove, K. Demeestere, S. Lenaerts, Appl. Catal. B-Environ. 106 (2011) 630–638.
[37] H.B. Huang, D.Q.D. Ye, Y.C. Leung, F.D. Feng, X.J. Guan, J. Mol. Catal. A-Chem. 336 (2011) 87–93.